The Journal of Chemical Physics ARTICLE scitation.org/journal/jcp

Examining the self-assembly of patchy alkane-grafted silica nanoparticles using molecular simulation

Cite as: J. Chem. Phys. 154, 034903 (2021); doi: 10.1063/5.0032658
Submitted: 9 October 2020 • Accepted: 14 December 2020 •
Published Online: 19 January 2021

Nicholas C. Craven,[1,2] Justin B. Gilmer,[1,2] Caroline J. Spindel,[2] Andrew Z. Summers,[2,3] Christopher R. Iacovella,[2,3] and Clare McCabe[2,3,4,a)]

AFFILIATIONS

[1]Interdisciplinary Materials Science Program, Vanderbilt University, Nashville, Tennessee 37235, USA
[2]Multiscale Modeling and Simulation (MuMS) Center, Vanderbilt University, Nashville, Tennessee 37235, USA
[3]Department of Chemical and Biomolecular Engineering, Vanderbilt University, Nashville, Tennessee 37235, USA
[4]Department of Chemistry, Vanderbilt University, Nashville, Tennessee 37235, USA

Note: This paper is part of the JCP Special Collection in Honor of Women in Chemical Physics and Physical Chemistry.
[a)]**Author to whom correspondence should be addressed:** c.mccabe@vanderbilt.edu

ABSTRACT

In this work, molecular dynamics simulations are used to examine the self-assembly of anisotropically coated "patchy" nanoparticles. Specifically, we use a coarse-grained model to examine silica nanoparticles coated with alkane chains, where the poles of the grafted nanoparticle are bare, resulting in strongly attractive patches. Through a systematic screening process, the patchy nanoparticles are found to form dispersed, string-like, and aggregated phases, dependent on the combination of alkane chain length, coating chain density, and the fractional coated surface area. Correlation analysis is used to identify the ability of various particle descriptors to predict bulk phase behavior from more computationally efficient single grafted nanoparticle simulations and demonstrates that the solvent-accessible surface area of the nanoparticle core is a key predictor of bulk phase behavior. The results of this work enhance our knowledge of the phase space of patchy nanoparticles and provide a powerful approach for future screening of these materials.

INTRODUCTION

The properties of systems containing nanoparticles are often highly correlated with the spatial arrangement of the underlying particles.[1–4] It has been demonstrated that the arrangement of nanoparticles is often dictated by the nanoparticle shape[5] and surface chemistry,[6] as well as the properties of the solvent or polymer matrix.[7] Functionalization of nanoparticles with oligomer or polymer coatings[8–10] is one method that has been demonstrated to allow control over nanoparticle arrangement and phase behavior. For example, Akcora *et al.* demonstrated via a combination of experiment, molecular simulation, and theory that the phase behavior of polystyrene grafted silica nanoparticles could be tuned through the modification of the length and density of the polystyrene grafts.[11] Long grafts and high surface densities resulted in the formation of dispersed nanoparticle phases, gradually transitioning to strings, sheets, and spherical aggregates as the graft length and/or graft density was reduced. The use of anisotropic surface functionalization allows further control over the phase behavior and structural arrangement of the nanoparticles by introducing directional interactions between nanoparticles. Often referred to as patchy particles, these anisotropic coatings can vastly increase the diversity and complexity of the structures formed by the nanoparticles.[12–16] For example, molecular simulations by Zhang *et al.* demonstrated that a variety of complex phases could be achieved by modifying the arrangement of attractive patches on the surface of simplified composite nanoparticles, including square-lattices, hexagonal-lattices, strings, rings, and polyhedral clusters.[17] Experiments by Fava *et al.* demonstrated that gold nanorods end-functionalized with polystyrene could be induced to form various phases depending on the solvent quality, including end-to-end, single-wide strings of nanorods when the solvent quality was good for the nanorods and spherical aggregates when the

solvent quality was poor for the nanorods.[18] DNA grafted nanoparticles have also been demonstrated as a means of creating highly specific, directional interactions between nanoparticles and colloids.[14,19,20] In other work, molecular simulations and theoretical calculations by Bianchi *et al.* demonstrated that significant changes to the liquid phase envelope could be achieved by the modification of the number of short range, directional, attractive patches on the spherical particles, where a reduction in the number of patches could be seen to increase the stability of the "liquid" regime to very low concentrations.[21]

Controlling the anisotropic effect for functionalized nanoparticles can be a complicated task as there is a nearly infinite design space of building blocks, where subtle features of the system (e.g., coating density, and length) may play a significant role in phase behavior. Molecular simulation enables the design space to be systematically probed by providing precise control over the individual building blocks and has been extensively used to study nanoparticle systems.[13,22–25] However, to date, most studies of nanoparticles with anisotropic interactions have used simplified, generic phenomenological models that represent the patchiness of the particles as differently interacting beads on a particle surface.[23,26,27] While such models have provided tremendous insight and relate well to patterning approaches used by experimentalists on larger length scales,[28] they do not necessarily relate to a specific chemistry and may not capture subtle details associated with polymer grafts (e.g., entropic interactions),[29,30] which may significantly impact the final structure/phase formed.[31] Grafted nanoparticle systems have also been studied via coarse-grained (CG) models, although limited work has considered anisotropic systems.[1,11,32–36] Furthermore, in most cases, these studies have utilized generic models of the chains and nanoparticle cores, rather than chemistry-specific[37–39] and, therefore, may not be directly relatable to specific chemistries.

Here, we examine the properties of patchy, grafted nanoparticles, using a chemistry-specific CG modeling approach. Nanoparticle interactions are governed by a CG model for silica nanoparticles developed in earlier work that was shown to accurately reproduce the energetic interactions of the corresponding atomistic models.[37] Surface coatings are modeled as alkane chains using the CG model of Nielsen *et al.* with implicit solvent interactions, where chains are considered to be in a good solvent and, thus, do no attract.[40] Uncoated regions of the nanoparticles result in the directional, attraction at the two poles. Using this detailed CG model, screening of the nanoparticle coatings is performed using the Molecular Simulation Design Framework (MoSDef),[41–45] to systematically examine the phase behavior of the nanoparticle systems, varying the density of the coating, fraction of surface coverage (FSA), and chain length of the alkane graft. The bulk phase behavior is used to plot phase diagrams to identify key relations between the screening parameters. Simulations of singular grafted nanoparticles are also performed and it is demonstrated that the solvent-accessible surface area (SASA) of the nanoparticle cores allows *a priori* prediction of the phase behavior of bulk systems.

SIMULATION DETAILS

Nanoparticle model

Patchy grafted nanoparticles are modeled as silica nanospheres, featuring an anisotropic (non-uniform) coating of alkane grafts. The CG model used to describe the nanoparticle cores was parameterized in earlier work to model silica.[36] The nanoparticles are constructed as a composite particle of beads arranged on a spherical surface using the golden spiral algorithm (see Fig. 1) following the work of

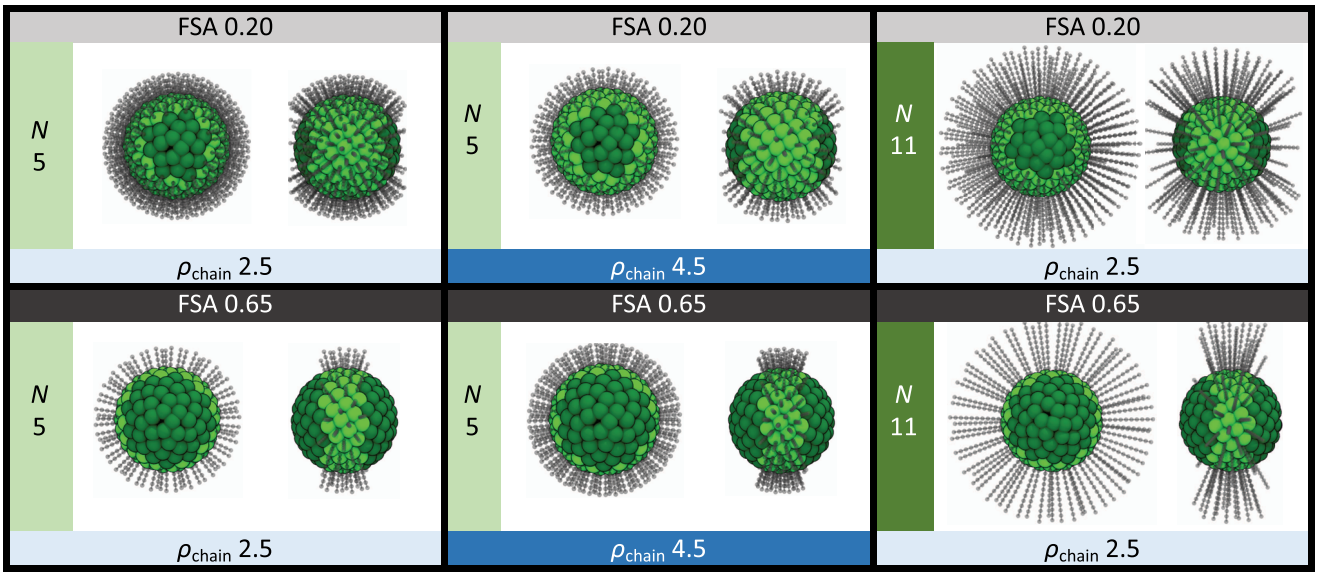

FIG. 1. Visualizations of grafted nanoparticles based on tunable model parameters of fractional surface area (FSA), chain length in CG beads (N), and chain density (ρ_{chain}). All grafted nanoparticles have symmetry about the equator and are shown in two different orientations. Light green beads represent CG silica beads attached to a CG alkane graft (gray). Dark green represents CG silica beads around the poles without grafts.

Summers *et al.*;[37] in all cases, the nanoparticles are modeled as 5.0 nm in diameter, with 153 CG beads. A Mie pair potential

$$U(r) = \left(\frac{n}{n-m}\right)\left(\frac{n}{m}\right)^{m/(n-m)} * \varepsilon\left[\left(\frac{\sigma}{r}\right)^{n} - \left(\frac{\sigma}{r}\right)^{m}\right] \quad (1)$$

was used to define the interaction between beads in the nanoparticles, where ε is the well depth and n and m are the potential exponents. This model of silica nanoparticles has been shown to accurately capture the energetic interactions between atomistic nanoparticles. We note that, while short range square well potentials are also widely used to model the interactions between nanoparticle cores in isotropically grafted nanoparticle simulations, Haley *et al.* demonstrated that the liquid phase envelope of polymer grafted nanoparticles was reduced as the range of the Lennard-Jones interaction between nanoparticle cores was reduced and began to more closely resemble a square well potential.[46] Similarly, Kalyuzhnyi *et al.* demonstrated that the liquid phase envelope of a four-site patchy particle model strongly depends on the core–core interactions. As such, accurately modeling these interactions is key for studying the assembly of nanoparticle systems.[47]

For alkane grafts, a 3:1 CG mapping from Nielsen *et al.* was used where single beads represent groupings of three methyl units.[40] Parameters for the interactions between the silica cores and the cross-interactions between silica cores and alkane grafts are derived to match interactions from all-atom models using the procedure outlined by Summers *et al.*[37] A schematic of a model grafted nanoparticle is included in Fig. S1 of the supplementary material, and all model parameters are reported in Table I. Bonds and angles for alkyl grafts are treated as harmonic bonds, with spring constants 1232.1 kcal/mol nm^2 and 2.8346 kcal/mol, respectively. The equilibrium length is set to 0.364 nm, and positions for angles are set for three chain groups to 3.019 42 radians and 3.054 33 radians for two chain groups and one terminus. Chains were constrained to the surface by a rigid bead; note that chains are not free to move about the surface of the nanoparticle and the nanoparticle core beads, and chain attachment beads, are integrated through time as a rigid body. The effects of solvent were treated implicitly through the use of a Langevin thermostat and by truncating chain–chain interactions at the minimum of the attractive well such that they are purely repulsive (i.e., the Weeks–Chandler–Andersen potential),[48] as has been done in prior studies.[37,49]

In this work, patchiness is introduced through a polar coating pattern where the grafted chains cover the surface of the silica core but are removed starting at the poles to expose the spherical core. This results in a band of grafts encircling the equator of the particle that varies in thickness. Three properties of the coating were investigated:

- Fractional surface area (FSA) of the exposed nanoparticle core, defined as the fraction of the nanoparticle core surface area that is not covered by alkane chains, i.e., the fraction of the nanoparticle that is "patchy."
- Chain density ρ_{chain} defined as chains per nanometer squared.
- Chain length N defined by the number of 3:1 CG alkane beads on each grafted chain.

The effect of the model parameters on the grafted nanoparticles can be seen in the visualizations in Fig. 1. Each grafted nanoparticle model was constructed using the mBuild library and parameterized with the Foyer library within the MoSDeF suite of tools.[41–43]

TABLE I. Mie interaction terms used to model CG nanoparticles and chains. Beads in the core are labeled "silica," beads along the length of the chain are labeled "chain," and beads that cap these chains are labeled "terminus."

Interactions	ε (kcal/mol)	σ (nm)	n	m
Silica–silica	0.928 6	0.6	20.0087	4.7578
Silica–chain	0.636 0	0.5291	29.6574	5.5835
Silica–terminus	0.678 8	0.5331	28.0821	5.6179
Chain–chain	0.389 092	0.4582	9.0	6.0
Terminus–terminus	0.434 996	0.4662	9.0	6.0
Chain–terminus	0.411 404	0.4662	9.0	6.0

Simulation and analysis details

Simulations were performed using the 1.3.3 version of the HOOMD-Blue molecular simulation engine[50,51] and the Signac framework for workflow management.[52,53] For bulk simulations, nanoparticle self-assembly was examined by placing 25 nanoparticles in a 40 × 40 × 40 nm^3 box for 100 ns, for a given set of design variables (see Table S1). In total 44 simulations (state points) were considered. The simulation workflow was as follows: First, a short energy minimization was performed to resolve any issues with overlapping particles from system construction, with a time step of 0.01 fs. This was followed by a 0.1 ns period to further relax the system, with a step size of 1 fs. Next, the system was annealed in four stages from 1000 K to 400 K, running for 10 ns with 4 fs time steps at each stage, to remove any dependence of the final self-assembled structure on the system's initial configuration. Finally, the system was run at 300 K for 50 ns, allowing a steady state configuration to be achieved. Data from the last 10 ns of the simulation were used for analysis. This analysis includes calculation of the radial distribution function (RDF), using the Freud Python package[54] analysis of local coordination using MDTraj,[55] and visualization using the visual molecular dynamics (VMD) package.[56]

Simulations of single grafted nanoparticles were also performed that screen over the range of chain length from 5 to 11 CG beads, chain density from 2.5 chains/nm^2 to 5.0 chains/nm^2, and FSA from 0.2 to 0.65, for a total of 539 simulations; 40 of these simulations correspond to the same design variables of the 44 bulk simulations. For each system, a brief energy minimization was performed followed by an NVT simulation run at 300 K for 10 ns with a 2 fs time step during which the nanoparticle core was held stationary, allowing only the alkane grafts to move. SASA was calculated with a 0.25 nm probe particle using MDTraj[55] and normalized by the idealized surface area of the 5.0 nm diameter nanoparticle (i.e., 2πD). The radius of gyration (R_g) of the entire grafted nanoparticle ($R_{g,gNP}$), R_g of each of the individual chains ($R_{g,chain}$), and asphericity of the entire grafted nanoparticle (i.e., including the core and chains) were calculated from the single particle trajectories using the MDAnalysis package.[57,58] To be consistent with other prior work,[12] we do not directly consider R_g but rather consider the ratio of nanoparticle

radius (2.5 nm) to the two R_g measures, which are labeled $R_{g,gNP}^{-1}$ and $R_{g,chain}^{-1}$. For analysis and comparison of the metrics computed in the bulk and single grafted nanoparticle simulations, Spearman's rank coefficients were determined using the SciPy computing package.[59]

RESULTS AND DISCUSSION

Bulk simulations

Simulations of bulk grafted nanoparticles were performed to examine the phase behavior as a function of chain length, surface grafted density, and FSA. The 44 systems simulated and the phases formed are listed in Table S1 of the supplementary material. Qualitatively, three distinct phases were observed, as shown in Fig. 2: dispersed, stringy, and aggregated. The phases were categorized both visually and by calculating the average number of nearest neighbors (i.e., the coordination number); nearest neighbors are defined as nanoparticles within a distance of 7.5 nm between the centers-of-mass of the nanoparticle core. Dispersed phases [Fig. 2(a)] are defined as those whose average nearest neighbor coordination number is less than 1. String-like aggregates [Fig. 2(b)] are defined as

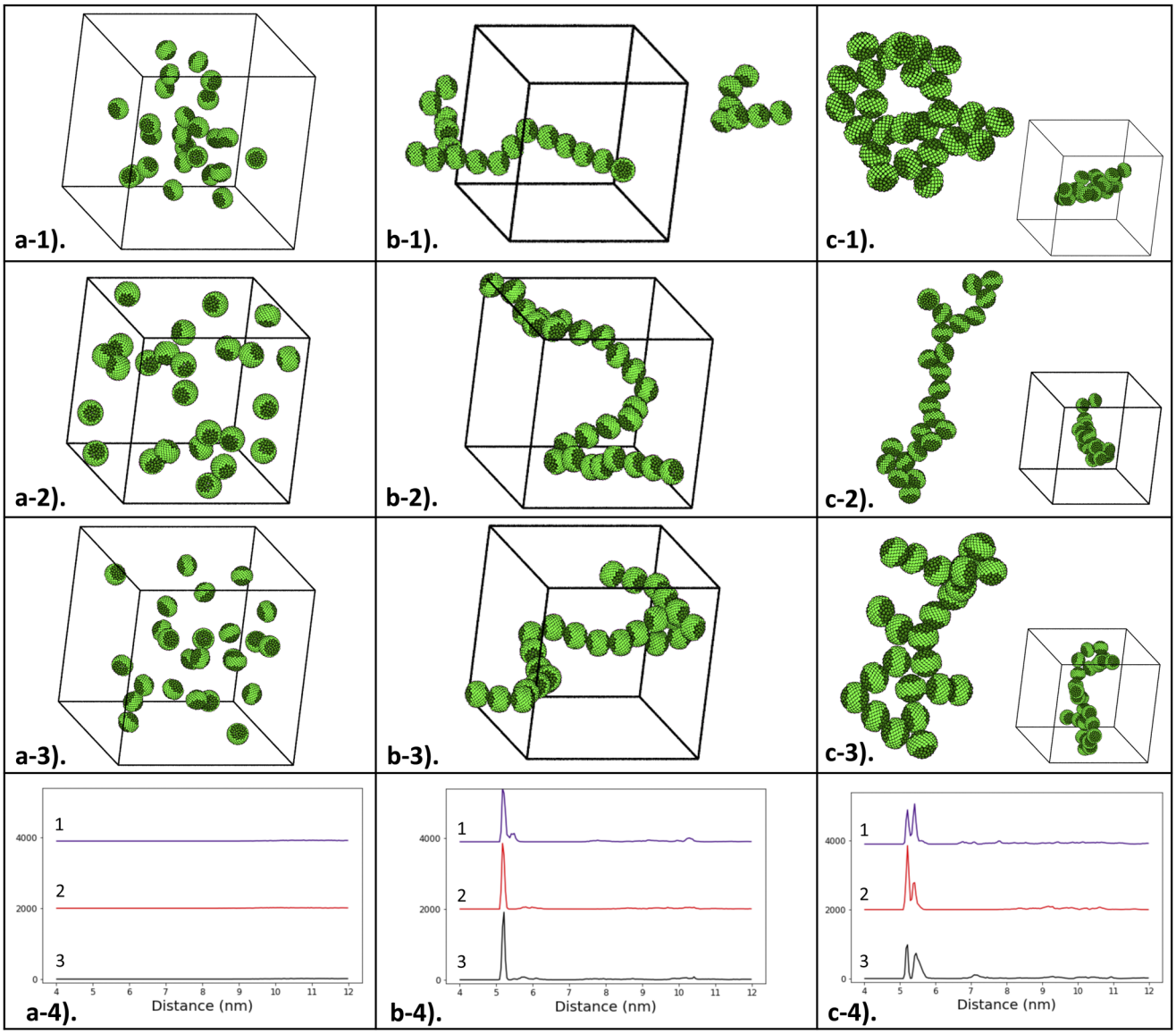

FIG. 2. Examples of equilibrium phases with coordination numbers of [(a1)–(a3)] 0.00, 0.00, 0.00 in the dispersed phase, [(b1)–(b3)] 1.80, 1.71, 1.76 in the stringy phase, and [(c1)–(c3)] 2.33, 2.41, 2.23 in the aggregated phase, respectively. (4) represents the corresponding RDFs to the visualized systems, offset by a value of 2000 in the y direction for clarity. Note that the scale of the RDFs is the same for all systems. Grafts are omitted for clarity in the visualizations. Figure S2 shows the same figure with grafted chains. Aggregated phases are visualized from two separate orientations to more clearly demonstrate the structure.

those with nearest neighbor coordination numbers ranging from 1 to 2 and a standard deviation of these values of less than one. The use of standard deviation ensures that systems that consist of multiple phases (e.g., higher-coordinated aggregated nanoparticles and lower-coordinated dispersed phases) are not misidentified as strings. The third phase observed is characterized by nanoparticles that aggregate but do not demonstrate significant string-like behavior or any long-range crystalline ordering [Fig. 2(c)]. Such phases are characterized by high coordination numbers; specifically, a coordination number greater than 2 is used to define an aggregated phase or those where the standard deviation is above 1. We note that, visually, the aggregated phases tend to be more planar in nature, rather than forming a spherical aggregate, as shown in Fig. 2(c). As evidenced by the coordination numbers (reported in the caption of Fig. 2 and Table S1 of the supplementary material), the dispersed phases show little-to-no aggregation of nanoparticles, whereas the aggregated phases show significant grouping, both at the un-coated poles and in the coated regions. This can also be seen in the radial distribution functions (RDFs) presented in the bottom row of Fig. 2, where dispersed phases do not show a strong first neighbor peak that would indicate aggregation, whereas the aggregated phases show two strong short-ranged peaks; the first peak corresponds to nanoparticles directly in surface contact at the patches, and the second peak, shifted by ~2 Å, corresponds to interactions between nanoparticles, buffered by the polymer grafts. A string-like phase appears as an intermediate between the dispersed and aggregated phases in which the nanoparticles aggregate, but only at the poles that are not grafted; this can be seen in Fig. 2(b–4). In general, the RDF of the string-like phase shows only a single peak at the first neighbor separation, corresponding to direct nanoparticle–nanoparticle contact, although strings that have multiple branches [see Figure 2(b–1)] show a small second peak shifted by ~2 Å.

To more clearly identify the correlations between chain density, chain length, FSA, and bulk phase, phase diagrams of the bulk systems studied are plotted in Figs. 3(a)–3(c). To simplify the ability to represent the data, one of the three variables (chain length, chain density, FSA) is held fixed, while the others are varied. From Fig. 3(a), it is clear that, for the fixed chain length of 6, phase behavior is most strongly linked to FSA and less dependent on chain density. Figure 3(b) shows that the likelihood of forming dispersed phases significantly increases as graft length increases and FSA decreases. For shorter chain lengths, as the FSA of the exposed nanoparticle core increases, nanoparticles begin to associate, first forming strings for moderate values, then transitioning to aggregate phases as the "patches" become larger and less localized. The phase behavior in Fig. 3(c) shows that nanoparticles with longer chain lengths and denser coatings are more likely to produce dispersed phases, as expected since such systems can more effectively shield the nanoparticle cores, while systems with shorter chain lengths and less dense coatings are more likely to form aggregate phases. The aforementioned work of Akcora *et al.* examined the phase behavior of isotropically grafted silica nanoparticles as a function of graft length and graft density, finding similar trends in terms of overall phase behavior as observed here.[11] We note that the string-like phases reported by Akcora *et al.* visually appear to be 1–2 nanoparticles in width, rather than the single nanoparticle-wide chains observed here, likely related to the more explicit directional interactions encoded in the patchy model. Additionally, we note that the aggregated phase observed in this work tends to a planar shape, in agreement with sheet-like structures observed by Akcora *et al.*; it was proposed that the underlying mechanism of sheet formation was kinetically controlled directional phase separation, supported by the analysis of the growth of the structures. It is likely that the same mechanism underlies the systems here, although our system sizes are too small to confidently quantify growth scaling. The simulation results reported herein are also in qualitative agreement with experiments of patchy spherical micelles formed from triblock copolymers that also formed string-like aggregates; such experiments considered the role of temperature and pH on the assembly, rather than grafting characteristics as reported herein, and thus, we cannot make a direct comparison of phase behavior.[16] We additionally note the clear agreement in terms of the formation of string-like phases in experiments

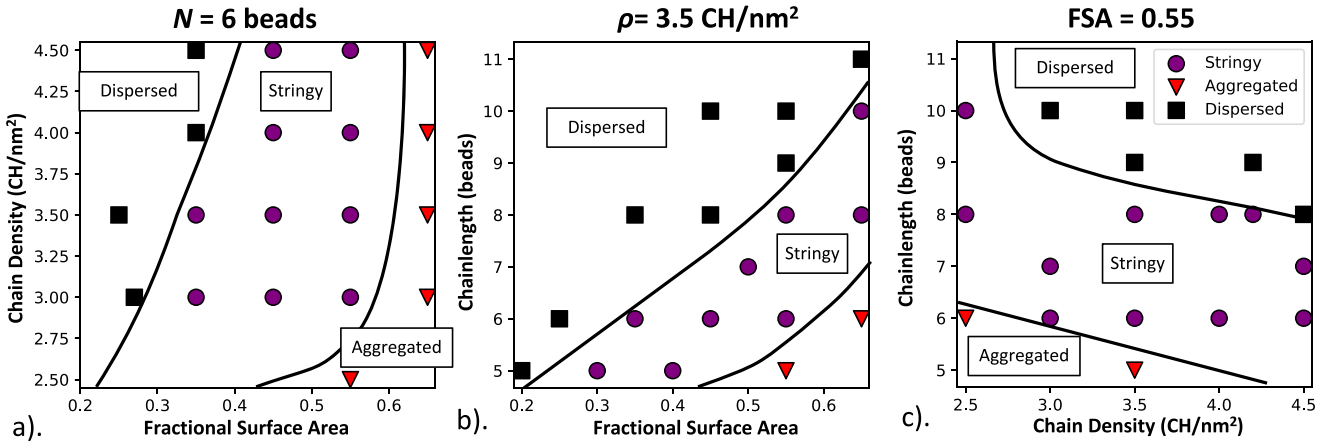

FIG. 3. Bulk phase diagrams for (a). ρ_{chain} as a function of FSA with N held constant at six beads, (b) FSA vs N with ρ_{chain} held constant at 3.5 chains/nm^2, (c) ρ_{chain} vs N with FSA held constant at 0.55. Black solid lines are to guide the eye, delineating the stringy, aggregated, and dispersed phases.

of larger, patchy colloids that assemble via charged patches at the poles.[28]

Single nanoparticle simulations

The literature contains several proposed metrics for relating bulk phase behavior to the properties of single grafted nanoparticles; the ability to predict phase landscapes from single nanoparticle simulations would allow for substantially reduced computational cost compared to bulk simulations. Specifically, Lafitte *et al.* related the asphericity of a single grafted nanoparticle to the bulk phase,[60] where it was found that grafted nanoparticles with low asphericity yielded dispersed phases and nanoparticles with increasing asphericity resulted in aggregated phases, with some stringy phases intermediate. This aggregation was proposed to result from reduced shielding of the attractive cores due to an uneven spread of grafted chains on the nanoparticle, which could be measured through asphericity.[61] Bozorgui *et al.* presented a geometric argument relating the radius of gyration (R_g) of the grafted chains to the radius of the particle, with regard to the ability of nanoparticle cores to achieve close contact. In subsequent related work, mean field theory calculations by Pryamtisyn *et al.* showed that the particle radius, normalized by R_g, of the grafted chains was a key parameter dictating the anisotropic assembly of grafted nanoparticles[12] (here, referred to by the variable $R^{-1}_{g,chain}$). In addition to these metrics, we consider R_g of the nanoparticle and chains, treated as a single entity, which implicitly captures some of the information of both asphericity and chain R_g; as discussed in the simulation details, we normalize the core nanoparticle radius by the R_g value of the nanoparticles and chains (here, referred to $R^{-1}_{g,gNP}$). To quantify the relative amount of the nanoparticle core that can be accessed, SASA is calculated and normalized by the nanoparticle surface area to give the fractional SASA (fSASA). We note that we would expect for short chains with dense surface coatings, fSASA should be closely related to FSA, and longer chains may act to shield the uncoated regions, reducing or completely eliminating access to the patches.

Spearman's rank correlation coefficients[62] were calculated to ascertain if correlations exist between (1) behavior observed for the bulk simulations (i.e., phase and the average and standard deviation of the coordination number), (2) system parameters (i.e., chain length, chain density, and FSA), and (3) properties measured from single grafted nanoparticle simulations (i.e., asphericity, $R^{-1}_{g,chain}$, $R^{-1}_{g,gNP}$, and fSASA). Figure 4 shows the correlations obtained, with larger and redder squares indicating correlations tending toward 1. Table S2 of the supplementary material reports the numerical values, while Figs. S3–S6 show the correlation scatter plots used to determine the correlation value. First, we can observe that the phase and coordination number (both average and standard deviation) are strongly correlated, as anticipated, given that this coordination number information was used to identify the bulk phase. We note that, individually, none of the system parameters are strongly correlated with phase information; this is as expected given that Fig. 3 clearly shows the multi-parameter dependence. Of the four metrics calculated for the single nanoparticle simulations, fSASA shows the largest correlation with phase. $R^{-1}_{g,gNP}$ and asphericity also appear to show reasonable correlation. $R^{-1}_{g,chain}$ does not appear strongly correlated with phase. We note that high correlation values do not necessarily indicate that the metric can be used in a predictive capacity. Figure 5 plots normalized histograms of various metrics as a function of the resulting bulk phase. Figure 5(a) considers fSASA, which

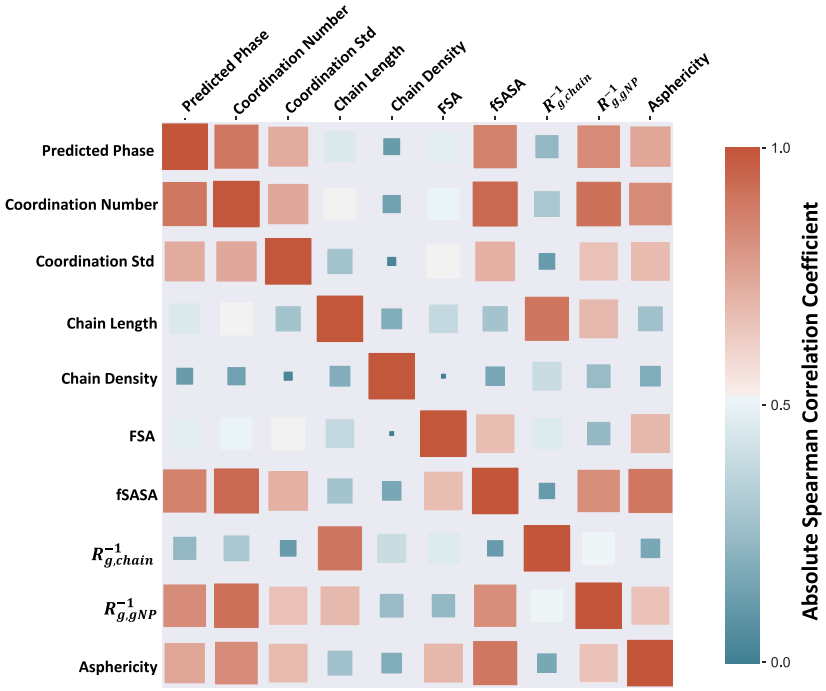

FIG. 4. Correlation matrix of key descriptors for the nanoparticle systems studied. Chain length, chain density, and FSA are explicitly defined parameters. Coordination number, coordination number standard deviation, and predicted phase are resultant measures from the bulk simulations. fSASA, $R^{-1}_{g,chain}$, $R^{-1}_{g,gNP}$, and asphericity are calculated from single nanoparticle simulations. $R^{-1}_{g,gNP}$ is defined as the nanoparticle radius divided by the radius of gyration of the grafted nanoparticle. $R^{-1}_{g,chain}$ is defined likewise, but with the radius of gyration of the grafts. Coefficient values close to unity correspond to stronger linear correlation, where strongly correlated systems are plotted as red, following the scale; note that the size of the markers also scales linearly with the correlation value.

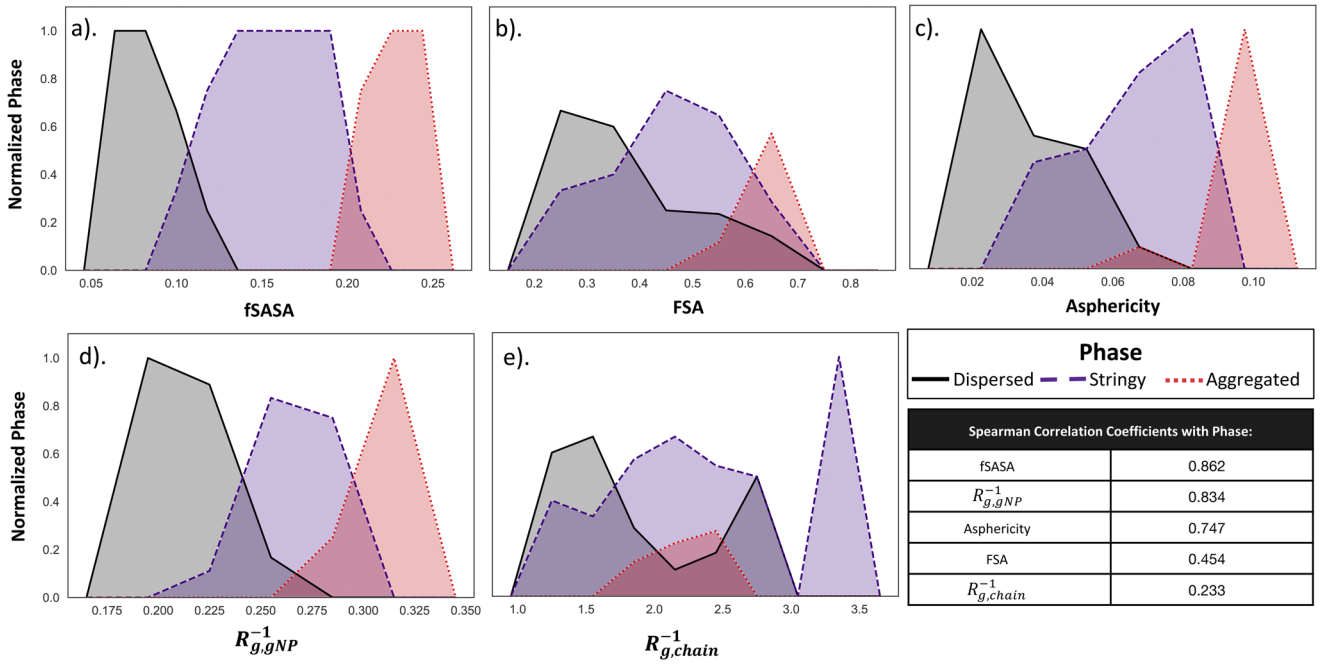

FIG. 5. Histograms of the fraction of simulations that result in a particular bulk phase binned by the metrics calculated from the single grafted nanoparticle simulations for (a) fSASA, (b) FSA, (c) asphericity (1 corresponds to a flat plane), (d) $R_{g,gNP}^{-1}$, and (e) $R_{g,chain}^{-1}$. Also included are Spearman's correlation coefficients of each parameter compared to the bulk phases reported. Higher correlation is an indication of better predictive nature using that metric.

again, demonstrated the strongest correlation with phase. While there is some overlap between histograms, each histogram is sufficiently unique, suggesting that fSASA can be used in a predictive capacity. For comparison, histograms of FSA are plotted in Fig. 5(b), where a substantial overlap is seen between each histogram, underscoring the need to use SASA to measure the actual patch area that is accessible. Figure 5(c) considers asphericity; even though significant correlations were observed with phase, it is clear that this metric is not sufficiently sensitive to uniquely identify each phase; only the highest asphericity values have a single unique phase associated with them. Figure 5(d) plots nanoparticle $R_{g,gNP}^{-1}$; while there appears to be clear correlations with phase, the overlap between histograms is larger than in the case of fSASA, where we note that there are no values of $R_{g,gNP}^{-1}$ that only result in a string-like phase, limiting the predictive power. However, $R_{g,gNP}^{-1}$ and asphericity may still be useful in helping to identify trends in the bulk phase behavior. $R_{g,chain}^{-1}$ is plotted in Fig. 5(e); substantial overlap between histograms is observed, and thus, as the correlation value suggests, this cannot be used in a predictive capacity for the systems considered here.

In order to test the ability of fSASA to be used in a predictive capacity for predicting phase behavior, heatmaps were constructed using a mesh algorithm from the fSASA values, as shown in Fig. 6; data points for the bulk phase systems, as reported in Fig. 3, are overlaid for comparison. Equivalent raw (i.e., unmeshed) heatmaps are included in Fig. S7 of the supplementary material. Here, a color gradient is defined to capture transition values, where white is used to capture the value of fSASA where the histograms cross in Fig. 5(a) (i.e., fSASA values of ~0.11 for dispersed to stringy and ~0.20 for stringy to aggregated), with the width of the gradients around these points correlating with the overlap of the histograms, suggestive of the uncertainty in identifying the phase. As such, regions of white can be considered to be estimates of the phase boundaries predicted by fSASA. Close agreement is seen between the phase behaviors predicted from fSASA calculated for the single grafted nanoparticle simulations in comparison with the phases identified from the bulk simulations. We note that the phase prediction in Fig. 6(c), where FSA is fixed at 0.55, shows a much more gradual transition from dispersed to stringy phases, as evidenced by the broad gradient. For a value of FSA = 0.55, most of the chains are distributed along the equator of the nanoparticle, with a large portion of the nanoparticle core exposed (e.g., see FSA = 0.65 in Fig. 1). In this regime (i.e., long chains and high FSA), chains will have a high degree of conformational freedom, which may result in larger variability in the measurement. Furthermore, the actual conformation may depend more strongly on the local environment of the grafted nanoparticle than for shorter chains with lower FSA, where chain conformations will likely change if they are near another nanoparticle (e.g., as discussed in the work of Bozorgui *et al.*[61] and Meng *et al.*[32]). The effects of interactions with neighbors are not captured by the single grafted nanoparticle simulations from which fSASA is calculated. Nonetheless, fSASA appears to be a strong predictor of phase. The supplementary material includes heatmaps generated from $R_{g,gNP}^{-1}$, $R_{g,chain}^{-1}$, and asphericity in Figs. S7–S12, including both raw and meshed histograms. As might be expected from Fig. 5, $R_{g,chain}^{-1}$ is not

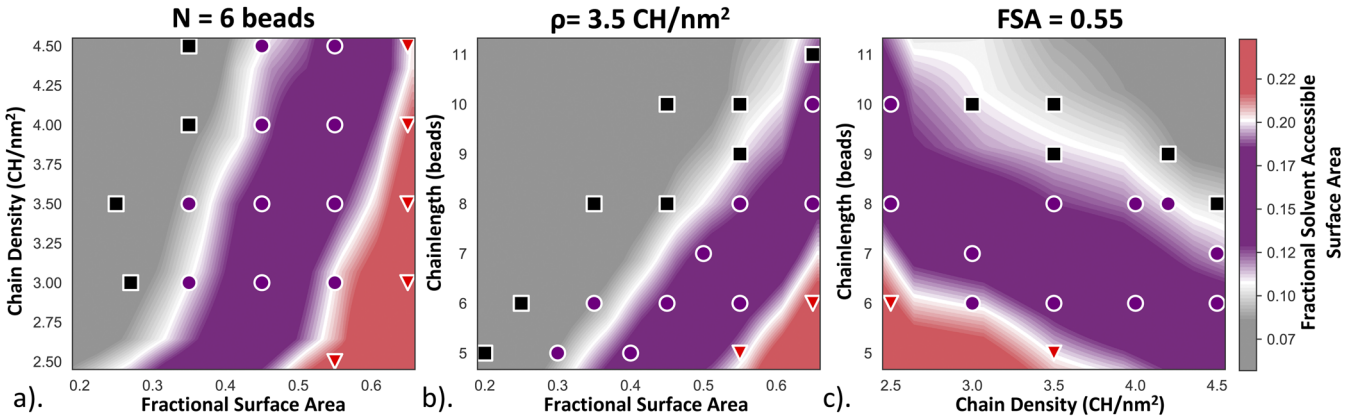

FIG. 6. Phase diagrams from Fig. 3 overlaid on fSASA heatmaps. White regions are mapped to the numerical value where histograms cross in Fig. 5(a). Bulk simulation phase is represented as black squares (dispersed phase), purple circles, (stringy phase), and red triangles (aggregated phase), following the same scheme in Fig. 3. Bilinear interpolation was used for meshing the fSASA heatmap values. (a) Chain density as a function of FSA with N held constant at six beads, (b) FSA vs N with chain density held constant at 3.5 chains/nm^2, (c) chain density vs N with FSA held constant at 0.55.

able to predict the phase behavior. $R_{g,gNP}^{-1}$ overall provides a reasonable estimate of the phase behavior, although, due to the overlap of the histograms, it does not provide as clear of a definition of the transitions as fSASA (i.e., the gradient regions are larger). Asphericity provides a reasonable estimate of phase behavior when considering phase as a function of FSA but does not seem to be predictive in the high FSA limit.

The results presented clearly demonstrate that for polar associating nanoparticle systems, fSASA values obtained from simulations of single nanoparticles offer insight into the phase of the corresponding bulk system and provide sufficient accuracy to be used in a predictive manner. As such, this may significantly reduce the need to run as many computationally intensive simulations of the corresponding bulk systems to establish a clear picture of the phase behavior. This may also allow for prescreening of the parameter space to identify regions of interest, again further reducing the computational cost of examining possible systems. As currently constructed, fSASA will not be able to help predict the structural arrangement for a particular coating pattern (e.g., that a hexagonal sheet would form by an equatorial pattern, as proposed by Zhang and Glotzer),[17] but it could help determine which combination of grafting variables are most likely to form the phase of interest (i.e., the region intermediate between low fSASA systems that will disperse and high fSASA systems that aggregate irrespective of the directional interactions).

CONCLUSION

Molecular dynamics simulations have been performed to study the self-assembly of grafted nanoparticles to gain insight into trends in phase behavior. A screening workflow was developed that leverages the MoSDeF toolkit for system building and parameterization, the management of this dataspace was handled by the Signac framework, and analysis was performed using MDTraj,[55] MDAnalysis,[57,58] and Freud.[54] Patchy alkane-grafted nanoparticles with chains excluded from the poles form three main phases: dispersed, stringy, and aggregated. Nanoparticle phases trend from dispersed, to stringy, to aggregated phases through the increased fractional surface area, decreased chain density, and reduced chain length. The fSASA of single-grafted nanoparticles was found to provide a predictive capability in terms of the equilibrium phase of the corresponding bulk systems of nanoparticles. Furthermore, the relationships explored in this work can likely be extended to other systems. For example, Asai *et al.* have shown that isotropic polymer grafted nanoparticles can behave like Janus particles due to surface fluctuations.[63] Although the explicit pattern patchy particles' display may be challenging to replicate, the general principles that determine the phase separation should be translatable to isotropic nanoparticles. While this work considered patches created by exposed nanoparticle cores, this analysis could be easily adapted to capture systems where directional attraction arises due to interactions between polymers. For example, we again note the close agreement between our work and that of patchy micelles formed from triblock copolymer building blocks;[16] we would anticipate that a similar fSASA analysis of model systems could be used to predict the phase behavior.

SUPPLEMENTARY MATERIAL

See the supplementary material for more information on all bulk simulation state point data, calculations of single particle descriptors, and additional plots of phase behavior and heatmaps. Also included is guidance to download and run the code used to analyze data and generate the figures.

AUTHORS' CONTRIBUTIONS

N.C.C. and J.B.G. contributed equally to this work.

DEDICATION

The authors dedicate this work to Carol K. Hall who is both a pioneer in the field and a steadfast supporter of women. She has supported the careers of countless women (including the corresponding author), whose careers would not have been possible without trailblazers like Carol for us to follow.

ACKNOWLEDGMENTS

The authors acknowledge support from the National Science Foundation through Grant No. OAC-1835874. The authors also thank the contributors to the MoSDeF project.

DATA AVAILABILITY

The data that support the findings of this study are openly available in a Zenodo database at https://zenodo.org/record/4042749, Ref. 64.

REFERENCES

[1]S. K. Kumar and R. Krishnamoorti, "Nanocomposites: Structure, phase behavior, and properties," Annu. Rev. Chem. Biomol. Eng. **1**(1), 37–58 (2010).
[2]S. Mann, "Self-assembly and transformation of hybrid nano-objects and nanostructures under equilibrium and non-equilibrium conditions," Nat. Mater. **8**(10), 781–792 (2009).
[3]A. Jayaraman, "Polymer grafted nanoparticles: Effect of chemical and physical heterogeneity in polymer grafts on particle assembly and dispersion," J. Polym. Sci., Part B: Polym. Phys. **51**(7), 524–534 (2013).
[4]S. Kadulkar, D. Banerjee, F. Khabaz, R. T. Bonnecaze, T. M. Truskett, and V. Ganesan, "Influence of morphology of colloidal nanoparticle gels on ion transport and rheology," J. Chem. Phys. **150**(21), 214903 (2019).
[5]S. Chen, R. S. Ingram, M. J. Hostetler *et al.*, "Gold nanoelectrodes of varied size: Transition to molecule-like charging," Science **280**(5372), 2098–2101 (1998).
[6]K.-S. Cho, D. V. Talapin, W. Gaschler, and C. B. Murray, "Designing PbSe nanowires and nanorings through oriented attachment of nanoparticles," J. Am. Chem. Soc. **127**(19), 7140–7147 (2005).
[7]M. Verma, K. Nehra, and P. S. Kumar, "Plasmonic oligomers: The role of polymer-solvent interactions," Adv. Sci. Lett. **22**(11), 3860–3862 (2016).
[8]M. Grzelczak, J. Vermant, E. M. Furst, and L. M. Liz-Marzán, "Directed self-assembly of nanoparticles," ACS Nano **4**(7), 3591–3605 (2010).
[9]C. Chevigny, F. Dalmas, E. Di Cola *et al.*, "Polymer-grafted-nanoparticles nanocomposites: Dispersion, grafted chain conformation, and rheological behavior," Macromolecules **44**(1), 122–133 (2011).
[10]S. Ekeroth, S. Ikeda, R. Boyd, P. Münger, T. Shimizu, and U. Helmersson, "Impact of nanoparticle magnetization on the 3D formation of dual-phase Ni/NiO nanoparticle-based nanotrusses," J. Nanopart. Res. **21**(11), 1–9 (2019).
[11]P. Akcora, H. Liu, S. K. Kumar *et al.*, "Anisotropic self-assembly of spherical polymer-grafted nanoparticles," Nat. Mater. **8**(4), 354–359 (2009).
[12]V. Pryamtisyn, V. Ganesan, A. Z. Panagiotopoulos, H. Liu, and S. K. Kumar, "Modeling the anisotropic self-assembly of spherical polymer-grafted nanoparticles," J. Chem. Phys. **131**(22), 221102 (2009).
[13]C. R. Iacovella, A. S. Keys, and S. C. Glotzer, "Self-assembly of soft-matter quasicrystals and their approximants," Proc. Natl. Acad. Sci. U. S. A. **108**(52), 20935–20940 (2011).
[14]É. Duguet, C. Hubert, C. Chomette, A. Perro, and S. Ravaine, "Patchy colloidal particles for programmed self-assembly," C. R. Chim. **19**(1-2), 173–182 (2016).
[15]R. M. Choueiri, E. Galati, H. Thérien-Aubin *et al.*, "Surface patterning of nanoparticles with polymer patches," Nature **538**(7623), 79–83 (2016).
[16]T.-L. Nghiem, T. I. Löbling, and A. H. Gröschel, "Supracolloidal chains of patchy micelles in water," Polym. Chem. **9**(13), 1583–1592 (2018).
[17]Z. Zhang and S. C. Glotzer, "Self-assembly of patchy particles," Nano Lett. **4**(8), 1407–1413 (2004).
[18]D. Fava, Z. Nie, M. A. Winnik, and E. Kumacheva, "Evolution of self-assembled structures of polymer-terminated gold nanorods in selective solvents," Adv. Mater. **20**(22), 4318–4322 (2008).
[19]W. Liu, N. A. Mahynski, O. Gang, A. Z. Panagiotopoulos, and S. K. Kumar, "Directionally interacting spheres and rods form ordered phases," ACS Nano **11**(5), 4950–4959 (2017).
[20]T. Tigges, T. Heuser, R. Tiwari, and A. Walther, "3D DNA origami cuboids as monodisperse patchy nanoparticles for switchable hierarchical self-assembly," Nano Lett. **16**(12), 7870–7874 (2016).
[21]E. Bianchi, P. Tartaglia, E. Zaccarelli, and F. Sciortino, "Theoretical and numerical study of the phase diagram of patchy colloids: Ordered and disordered patch arrangements," J. Chem. Phys. **128**(14), 144504 (2008).
[22]J. Kalb, D. Dukes, S. K. Kumar, R. S. Hoy, and G. S. Grest, "End grafted polymernanoparticles in a polymeric matrix: Effect of coverage and curvature," Soft Matter **7**(4), 1418–1425 (2011).
[23]C. R. Iacovella and S. C. Glotzer, "Phase behavior of ditethered nanospheres," Soft Matter **5**(22), 4492 (2009).
[24]T. V. M. Ndoro, E. Voyiatzis, A. Ghanbari, D. N. Theodorou, M. C. Böhm, and F. Müller-Plathe, "Interface of grafted and ungrafted silica nanoparticles with a polystyrene matrix: Atomistic molecular dynamics simulations," Macromolecules **44**(7), 2316–2327 (2011).
[25]G. D. Hattemer and G. Arya, "Viscoelastic properties of polymer-grafted nanoparticle composites from molecular dynamics simulations," Macromolecules **48**(4), 1240–1255 (2015).
[26]Z. Zhang, M. A. Horsch, M. H. Lamm, and S. C. Glotzer, "Tethered nano building blocks: Toward a conceptual framework for nanoparticle self-assembly," Nano Lett. **3**(10), 1341–1346 (2003).
[27]C. R. Iacovella and S. C. Glotzer, "Complex crystal structures formed by the self-assembly of ditethered nanospheres," Nano Lett. **9**(3), 1206–1211 (2009).
[28]P. Song, Y. Wang, Y. Wang *et al.*, "Patchy particle packing under electric fields," J. Am. Chem. Soc. **137**(8), 3069–3075 (2015).
[29]C. Singh, P. K. Ghorai, M. A. Horsch *et al.*, "Entropy-mediated patterning of surfactant-coated nanoparticles and surfaces," Phys. Rev. Lett. **99**(22), 226106 (2007).
[30]Z. Liu, R. Guo, G. Xu, Z. Huang, and L.-T. Yan, "Entropy-mediated mechanical response of the interfacial nanoparticle patterning," Nano Lett. **14**(12), 6910–6916 (2014).
[31]A. H. Gröschel, A. Walther, T. I. Löbling, F. H. Schacher, H. Schmalz, and A. H. E. Müller, "Guided hierarchical co-assembly of soft patchy nanoparticles," Nature **503**(7475), 247–251 (2013).
[32]D. Meng, S. K. Kumar, J. M. D. Lane, and G. S. Grest, "Effective interactions between grafted nanoparticles in a polymer matrix," Soft Matter **8**(18), 5002 (2012).
[33]T. B. Martin, A. Seifpour, and A. Jayaraman, "Assembly of copolymer functionalized nanoparticles: A Monte Carlo simulation study," Soft Matter **7**(13), 5952 (2011).
[34]T. C. Moore, C. R. Iacovella, and C. McCabe, "Derivation of coarse-grained potentials via multistate iterative Boltzmann inversion," J. Chem. Phys. **140**(22), 224104 (2014).
[35]K. Shi, E. E. Santiso, and K. E. Gubbins, "Bottom-up approach to the coarse-grained surface model: Effective solid-fluid potentials for adsorption on heterogeneous surfaces," Langmuir **35**(17), 5975–5986 (2019).
[36]A. Chremos, A. Z. Panagiotopoulos, H.-Y. Yu, and D. L. Koch, "Structure of solvent-free grafted nanoparticles: Molecular dynamics and density-functional theory," J. Chem. Phys. **135**(11), 114901 (2011).
[37]A. Z. Summers, C. R. Iacovella, O. M. Cane, P. T. Cummings, and C. McCabe, "A transferable, multi-resolution coarse-grained model for amorphous silica nanoparticles," J. Chem. Theory Comput. **15**(5), 3260–3271 (2019).
[38]L. Cheng and D. Cao, "Aggregation of polymer-grafted nanoparticles in good solvents: A hierarchical modeling method," J. Chem. Phys. **135**(12), 124703 (2011).

[39]E. R. Chan, A. Striolo, C. McCabe, P. T. Cummings, and S. C. Glotzer, "Coarse-grained force field for simulating polymer-tethered silsesquioxane self-assembly in solution," J. Chem. Phys. **127**(11), 114102 (2007).
[40]S. O. Nielsen, C. F. Lopez, G. Srinivas, and M. L. Klein, "A coarse grain model for n-alkanes parameterized from surface tension data," J. Chem. Phys. **119**(14), 7043 (2003).
[41]MoSDeF home page.
[42]C. Klein, J. Sallai, T. J. Jones, C. R. Iacovella, C. McCabe, and P. T. Cummings, "A hierarchical, component based approach to screening properties of soft matter," in *Foundations of Molecular Modeling and Simulation* (Springer, 2016), pp. 79–92.
[43]C. Klein, A. Z. Summers, M. W. Thompson *et al.*, "Formalizing atom-typing and the dissemination of force fields with foyer," Comput. Mater. Sci. **167**, 215–227 (2019).
[44]A. Z. Summers, J. B. Gilmer, C. R. Iacovella, P. T. Cummings, and C. MCabe, "MoSDeF, a Python framework enabling large-scale computational screening of soft matter: Application to chemistry-property relationships in lubricating monolayer films," J. Chem. Theory Comput. **16**(3), 1779–1793 (2020).
[45]M. W. Thompson, J. B. Gilmer, R. A. Matsumoto *et al.*, "Towards molecular simulations that are transparent, reproducible, usable by others, and extensible (TRUE)," Mol. Phys. **118**, e1742938 (2020).
[46]J. D. Haley, C. R. Iacovella, P. T. Cummings, and C. McCabe, "Examining the aggregation behavior of polymer grafted nanoparticles using molecular simulation and theory," J. Chem. Phys. **143**(5), 054904 (2015).
[47]Y. V. Kalyuzhnyi, C. R. Iacovella, H. Docherty, M. Holovko, and P. T. Cummings, "Network forming fluids: Yukawa square-well m-point model," J. Stat. Phys. **145**(2), 481–506 (2011).
[48]J. D. Weeks, D. Chandler, and H. C. Andersen, "Role of repulsive forces in determining the equilibrium structure of simple liquids," J. Chem. Phys. **54**(12), 5237–5247 (1971).
[49]B. L. Peters, J. M. D. Lane, A. E. Ismail, and G. S. Grest, "Fully atomistic simulations of the response of silica nanoparticle coatings to alkane solvents," Langmuir **28**(50), 17443–17449 (2012).
[50]J. Glaser, T. D. Nguyen, J. A. Anderson *et al.*, "Strong scaling of general-purpose molecular dynamics simulations on GPUs," Comput. Phys. Commun. **192**, 97–107 (2015).
[51]J. A. Anderson, C. D. Lorenz, and A. Travesset, "General purpose molecular dynamics simulations fully implemented on graphics processing units," J. Comput. Phys. **227**(10), 5342–5359 (2008).
[52]C. S. Adorf, P. M. Dodd, V. Ramasubramani, and S. C. Glotzer, "Simple data and workflow management with the signac framework," Comput. Mater. Sci. **146**, 220–229 (2018).
[53]C. S. Adorf, V. Ramasubramani, B. D. Dice, M. M. Henry, P. M. Dodd, and S. C. Glotzer (2019). "glotzerlab/signac," Zenodo. http://doi.org/10.5281/zenodo.2581327
[54]V. Ramasubramani, B. D. Dice, E. S. Harper, M. P. Spellings, J. A. Anderson, and S. C. Glotzer, "freud: A software suite for high throughput analysis of particle simulation data," Comput. Phys. Commun. **254**, 107275 (2020).
[55]R. T. Mcgibbon, K. A. Beauchamp, M. P. Harrigan *et al.*, "Computational tools MDTraj: A modern open library for the analysis of molecular dynamics trajectories," Biophys J. **109**, 1528–1532 (2015).
[56]W. Humphrey, A. Dalke, and K. Schulten, "VMD: Visual molecular dynamics," J. Mol. Graphics **14**(1), 33–38 (1996).
[57]N. Michaud-Agrawal, E. J. Denning, T. B. Woolf, and O. Beckstein, "MDAnalysis: A toolkit for the analysis of molecular dynamics simulations," J. Comput. Chem. **32**(10), 2319–2327 (2011).
[58]R. J. Gowers, M. Linke, J. Barnoud *et al.*, MDAnalysis: A Python package for the rapid analysis of molecular dynamics simulations, 2016.
[59]P. Virtanen, R. Gommers, T. E. Oliphant *et al.*, "SciPy 1.0: Fundamental algorithms for scientific computing in Python," Nat. Methods **17**(3), 261–272 (2020).
[60]T. Lafitte, S. K. Kumar, and A. Z. Panagiotopoulos, "Self-assembly of polymer-grafted nanoparticles in thin films," Soft Matter **10**(5), 786–794 (2014).
[61]B. Bozorgui, D. Meng, S. K. Kumar, C. Chakravarty, and A. Cacciuto, "Fluctuation-driven anisotropic assembly in nanoscale systems," Nano Lett. **13**(6), 2732–2737 (2013).
[62]D. Zwillinger and S. Kokoska, *CRC Standard Probability and Statistics Tables and Formulae* (CRC Press, 1999).
[63]M. Asai, A. Cacciuto, and S. K. Kumar, "Quantitative analogy between polymer-grafted nanoparticles and patchy particles," Soft Matter **11**(4), 793–797 (2015).
[64]N. Craven, J. Gilmer, C. Spindel, A. Summers, C. Iacovella, and C. McCabe (2020). "Examining the self-assembly of patchy alkane-grafted silica nanoparticles using molecular simulation," Zenodo. http://doi.org/10.5281/zenodo.4042749